Supporting Information for the article

Searching for relevant criteria to distinguish natural *vs.* anthropogenic TiO$_2$ nanoparticles in soils

Ana Elena Pradas del Real, Hiram Castillo-Michel, Ralf Kaegi, Camille Larue, Wout de Nolf, Juan Reyes-Herrera, Rémi Tucoulou, Nathaniel Findling[a] , Eduardo Salas-Colera and Géraldine Sarret

Materials and methods

1. Elemental analyses by ICP-MS

Approximately 200 mg of dried soil were introduced in Teflon tubes together with a mixture of acids (2 mL HNO$_3$, 1 mL HClO$_4$, 1 mL NH$_4$F) and heated at 100 °C (cap closed). After 2 hours, 1 mL of H$_2$O$_2$ was added and the solution was heated for one more hour. After introduction of an additional 1 mL of HNO$_3$, the tubes were left open in the heating system (at 100°C) until near complete evaporation. This step (addition of HNO$_3$ and evaporation) was reproduced two more times. Finally 1 mL of ultrapure H$_2$O was added and the tubes were further heated for 30 min (cap closed). Samples were diluted using 5% HNO$_3$ and ICP-MS measurements were done using magnetic sector field HR ICP-MS (High Resolution Inductively Coupled Plasma Mass Spectrometry, Element XR) in the Service ICP-MS of the Observatoire Midi-Pyrénées (Toulouse). Instrumental calibration was processed every 6-8 samples of an analytical run by 3 dilutions of a certified NIST standard. Each sample was measured three times (three technical replicates). Measurement quality was assessed by analyzing a certified reference material of rainwater (TMRAIN-04). Results were always within a 10% confidence interval around the certified value.

2. Particle size distribution analysis

This procedure was done using ImageJ [1] by adapting protocols developed for transmission electron microscopy (TEM) images, for instance [2]. All criteria used were first tested and validated on a selected zone of the nanoXRF map.

2.1. Image preprocessing. Three images were generated from each nanoXRF map, with different selections of the grayscale range width (full width, 90% and 80%). Note that the lower levels were always included, otherwise there was a clear degradation of the image (Figure S1).
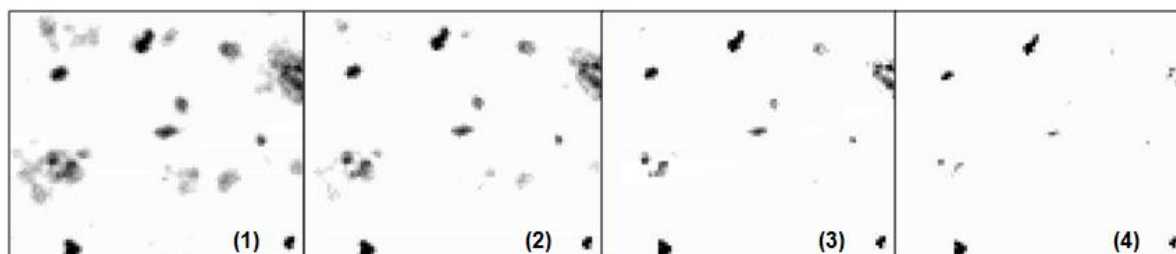
Figure S1. Particle area degradation examples by cutting the lower gray levels of a selected frame from a nanoXRF map. (1) Original: 0-100% and three different windows, all with a 80% grayscale width selection : (2) Window:5%-85% (3) Window: 10%-90% and (4) Window: 15%-95%.
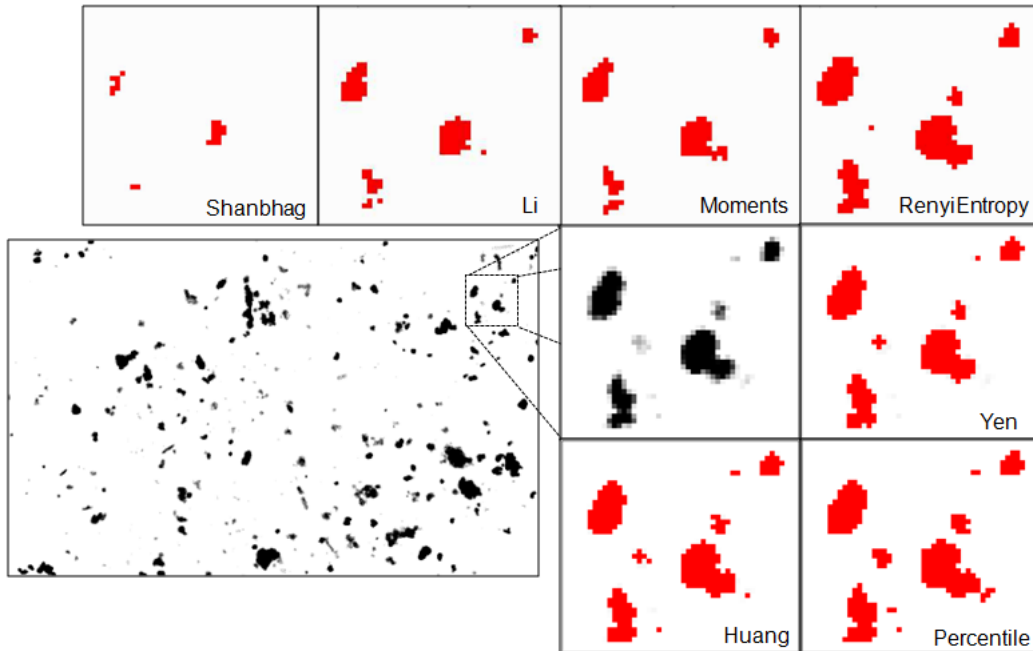
Figure S2. Comparison of results obtained with different auto-threshold routines.

2.2. Threshold routines. Two auto-thresholds routines available in ImageJ were applied, the Yen [3] and the Huang [4] ones. These two routines provided the more accurate number of particles, as tested for a small portion of the sludge maps (Figure S2). The Yen routine slightly underestimated the number of particles, and Huang slightly overestimated them (Figure S2). Therefore, Yen and Huang counts for 3 grayscale ranges (full width, 90% and 80%) were averaged and used to calculate the statistical uncertainty. Results of all routines available in ImageJ are shown in Figure S3.

Figure S3. Total number of particles obtained for the entire sludge map from each auto-threshold routine, sorted from smallest to largest.

2.3. Despeckle filter. The ImageJ despeckle filter was then applied, in order to remove single pixel artefacts resulting from the threshold operation (Figure S4).
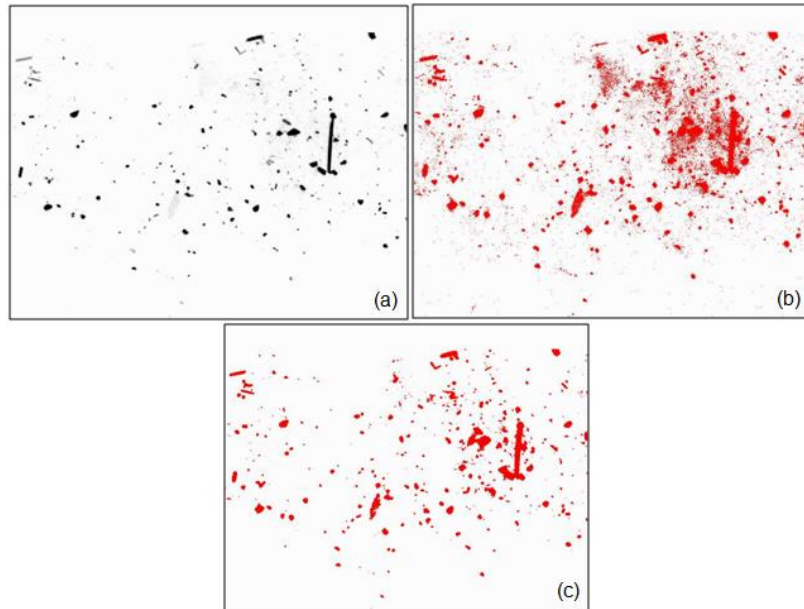
Figure S1. (a) Original image of the sludge-amended soil (b) Many single pixel artefacts appeared after the Huang threshold process (c) Huang threshold after applying the despeckle filter.

2.4. Feret diameter. The particles do not have a perfect circular shape. The Feret diameter, i.e., the distance between two parallel tangents on opposite sides of the image of a particle, is a suitable length to describe the particle size (Figure S5). In this work, the reported diameter is the average of the maximum and minimum Feret diameter.
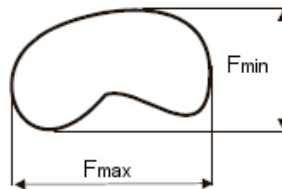
Figure S2. Maximum Feret diameter (Fmax) and minimum (Fmin) of an irregular shape particle, both magnitudes are given by ImageJ.

2.5. Diameter categories. The Nyquist criterion specifies that the image sampling interval must be smaller than half the desired resolution [5]. Therefore, in this work, a 100 nm (two pixels) resolution was appropriate to categorize the particle size distribution. Four categories were defined, < 100 nm, 100-200 nm, 200-300 and > 300 m.

2.6. Limitations of the method. The particle size distribution obtained by image analysis is often affected by the presence of aggregates or agglomerates. In the present work, none of the used thresholds were able to separate particles that were too close, therefore aggregates were treated as single particle (Figure S6). Thus, this type of analysis likely overestimates the number of larger particles.
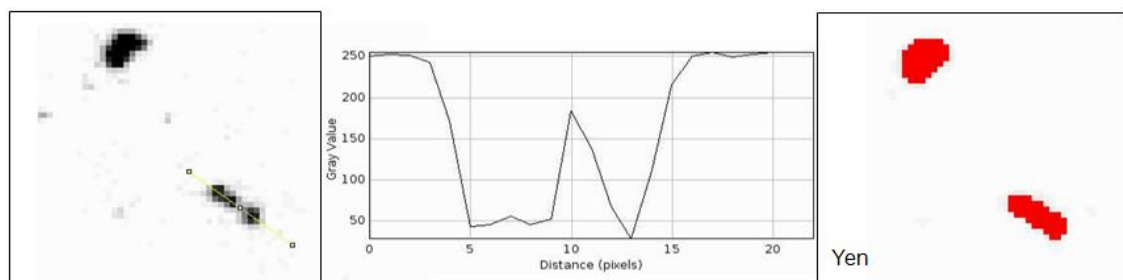
Figure S6. Example of how the threshold process cannot separate close particles, and considers the aggregate as a single, larger particle.

References

[1]   Rueden, C. T.; Schindelin, J. & Hiner, M. C. et al., *ImageJ2: ImageJ for the next generation of scientific image data*, BMC Bioinformatics 18 (2017) 529, doi:10.1186/s12859-017-1934-z.

[2]   Rice, S. B. et al., *Particle size distributions by transmission electron microscopy: an interlaboratory comparison case study*, Metrologia 50 (2013) 663-678, doi:10.1088/0026-1394/50/6/663.

[3]   Yen J. C., Chang F. J., Chang S (1995), *A New Criterion for Automatic Multilevel Thresholding*, IEEE Trans. on Image Processing 4 (3): 370-378, ISSN 1057-7149, doi:10.1109/83.366472.

[4]   Huang L. K. and Wang M.J., *Image thresholding by minimizing the measures of fuzziness*, Patter Recognition 28 (1995) 41-51.

[5]   Shroff, H. et al., Live-cell photoactivated localization microscopy of nanoscale adhesion dynamics, Nature Methods 5 (2008) 417-423, doi:10.1038/nmeth.1202.

Results

Table S1. Elemental concentrations determined by ICP-MS in the soil, sludge and sludge-amended soil

		g kg^{-1}											mg kg^{-1}													
		Na	Mg	Al	Si	P	S	K	Ca	Ti	Fe	Mn	Cr	Co	Ni	Cu	Zn	Ga	Cd	Sn	Sb	Pb	Cs	Ba	La	Ce
soil	mean	5.6	3.8	21.6	41.5[a]	0.9	0.4	7.0	4.1	0.79	15.8	0.77	34.9	5.2	16.6	12.6	42.7	6.8	0.3	7.5	0.6	28.9	3.8	182.6	5.9	15.3
	SD	0.4	0.4	2.7	-	0.1	0.0	0.4	0.2	0.11	0.6	0.07	0.9	0.3	0.7	1.1	1.4	0.9	0.0	0.8	0.1	3.4	1.3	17.5	2.0	4.3
sludge	mean	5.5	5.8	5.8	3.4	19.0	10.6	3.6	68.0	0.46	14.4	0.33	67.4	4.9	53.0	505.2	734.8	2.2	1.1	52.7	2.5	28.4	0.8	342.9	4.8	9.1
	SD	0.4	1.0	1.6	0.3	2.2	0.1	0.4	8.4	0.11	2.0	0.04	5.9	0.5	4.8	59.2	85.2	0.3	0.2	12.7	0.2	3.1	0.1	38.8	0.7	1.4
soil+sludge	mean	6.2	3.9	18.8	37.7	3.0	1.9	7.1	9.5	0.80	15.6	0.75	38.6	5.2	20.1	67.5	121.3	6.0	0.4	15.9	1.0	29.8	2.2	233.2	11.1	23.0
	SD	0.4	0.3	3.6	2.0	0.5	1.2	1.6	1.6	0.15	3.2	0.15	7.8	1.1	3.8	11.0	19.5	1.2	0.1	2.2	0.2	4.9	0.4	33.9	3.4	4.6
soil+sludge, calc.[b]		5.6	4.0	20.0		2.7	1.4	6.7	10.5	0.76	15.6	0.73	38.2	5.2	20.3	61.9	111.9	6.4	0.3	12.0	0.8	28.9	3.5	198.6	5.8	14.6
		0.4	0.4	2.6		0.3	0.0	0.4	1.0	0.11	0.7	0.07	1.4	0.3	1.1	6.9	9.8	0.8	0.0	2.0	0.1	3.4	1.2	19.7	1.8	4.0

Mean and SD calculated on the analysis of three replicate samples. a calculated from the sludge and soil+sludge concentrations. b calculated from the soil and sludge concentrations

Table S1, cont.. calculated Ba/Ti and Ce/Ti elemental ratios

	Ba/Ti	Ce/Ti
soil	0.23	0.02
sludge	0.75	0.02
soil+sludge	0.29	0.03
soil+sludge, calc.[b]	0.26	0.02

Table S2 . Ti species distribution (in molar % of Ti) in sewage sludge and soil bulk samples (spectra shown in Figure 5) obtained by Linear Least squares Combination Fitting.

| | Ti species | | | | |
Sample	Anatase	Rutile	Amorph. TiO$_2$	Sum	*R factor*
Sludge_bulk1	54	47	0	101	9.70E-04
Sludge_bulk2	55	45	0	100	7.80E-04
Sludge_bulk3	55	43	0	98	6.59E-04
Soil_bulk1	36	57	7	100	1.92E-03
Soil_bulk2	40	43	17	100	1.57E-04
Soil_bulk3	36	47	17	100	1.10E-04
Soil+sludge_bulk1	39	42	21	102	3.02E-04
Soil+sludge_bulk3	23	43	34	100	2.20E-04

R factor: Residual between fit and experimental data = $\Sigma[\mu_{exp} - \mu_{fit}]^2 / \Sigma[\mu_{exp}]^2$, where μ is the normalized absorbance.

Table S3 . Ti species distribution (in molar % of Ti) in sewage sludge obtained by Linear Least squares Combination Fitting of Ti K-edge μXANES spectra shown in Figure 6.

| | Ti species | | | | |
Sample	Anatase	Rutile	Amorph. TiO$_2$	Sum	*R factor*
sludge 1.3 fXAS 7	20	75	0	95	2.19E-03
sludge 1.3 fXAS 5	44	40	16	100	1.94E-03
sludge 1.3 fXAS 6	73	28	0	101	5.00E-04
sludge 1.3 average	46	56	0	102	1.22E-03
point1	11	93	0	104	8.00E-04
point2	82	0	19	101	1.06E-03
point3	0	100	0	100	1.70E-04
point4	21	84	0	105	4.12E-03
point5	100	0	0	100	6.10E-04
sludge 1.1 fXAS 1	100	0	0	100	2.65E-03
sludge 1.1 fXAS 2	60	38	0	98	1.75E-03
sludge 1.1 average	47	44	11	102	1.79E-03
sludge 1.2 fXAS 3	71	10	18	99	3.99E-03
sludge 1.2 fXAS 4	100	0	0	100	2.25E-03
sludge 1.2 average	62	41	0	103	5.97E-04

R factor: Residual between fit and experimental data = $\Sigma[\mu_{exp} - \mu_{fit}]^2 / \Sigma[\mu_{exp}]^2$, where μ is the normalized absorbance.

Table S4 . Ti species distribution (in molar % of Ti) in sewage sludge obtained by Linear Least squares Combination Fitting of Ti K-edge μXANES spectra shown in Figure S10 and S11.

Sample	Ti species			Sum	R factor
	Anatase	Rutile	Amorph. TiO$_2$		
sludge SI-2.1 average	27	68	0	68	2.40E-03
sludge SI-2.2 average	32	65	0	65	4.00E-04
sludge SI-2.2 fXAS1	9	86	0	86	1.30E-03
sludge SI-2.2 fXAS2	0	100	0	100	1.20E-03
sludge SI-2.2 fXAS3	47	49	0	49	7.20E-04
sludge SI-2 average	65	25	0	25	6.00E-03
sludge SI-2 fXAS1	53	42	0	42	7.00E-03
sludge SI-3.1 average	47	49	0	49	5.80E-04
sludge SI-3.2 average	86	11	0	11	1.90E-03
sludge SI-3.3 average	56	28	9	37	1.88E-03
sludge SI-3.3 fXAS1	84	11	0	11	5.00E-03
sludge SI-3.3 fXAS2	80	14	0	14	2.40E-03
sludge SI-3.3 fXAS3	68	32	0	32	3.40E-03
sludge SI-3.4 average	47	41	0	41	4.70E-03
sludge SI-3.4 fXAS1	27	71	0	71	6.70E-03
sludge SI-3.4 fXAS2	78	9	0	9	5.20E-03
sludge SI-3.4 fXAS3	43	44	0	44	6.10E-03
sludge SI-3.4 rem	55	42	0	42	4.00E-03
sludge SI-3.5 average	22	74	0	74	2.00E-03
sludge SI-3.5 fXAS1	15	82	0	82	1.80E-03
sludge SI-3.5 fXAS2	9	69	0	69	3.30E-03
sludge SI-3.6 average	47	30	18	48	6.60E-04
sludge SI-3.6 fXAS1	71	13	10	23	1.30E-03
sludge SI-3.6 fXAS2	30	38	27	65	5.90E-04
sludge SI-3.6 fXAS3	52	36	7	43	6.70E-04
sludge SI-3.7 average	47	42	6	48	5.30E-04
sludge SI-3.7 fXAS1	51	30	13	43	1.30E-03
sludge SI-3.7 fXAS2	50	47	0	47	5.40E-04
sludge SI-3.7 fXAS3	34	49	12	61	9.60E-04
sludge SI-3.7 fXAS4	48	48	0	48	5.70E-04
sludge SI-3.8 average	21	41	33	74	8.50E-04
sludge SI-3.9 average	42	40	13	53	9.70E-04
sludge SI-3.9 fXAS1	42	51	0	51	1.30E-03
sludge SI-3.9 fXAS2	47	35	13	48	6.70E-04
sludge SI-3.9 fXAS3	62	15	22	37	2.20E-03
sludge SI-3.9 fXAS4	47	37	11	48	7.90E-04
sludge SI-3.9 fXAS5	31	38	25	63	1.80E-03
sludge SI-3.9 fXAS6	47	31	17	48	1.20E-03
sludge SI-4.1 average	43	50	0	50	8.00E-04
sludge SI-4.1 fXAS1	17	82	0	82	1.20E-03
sludge SI-4.1 fXAS2	31	67	0	67	1.40E-03
sludge SI-4.1 fXAS3	42	56	0	56	5.70E-04
sludge SI-4.1 fXAS4	36	60	18	78	8.90E-04
sludge SI-4.1 fXAS5	36	43	0	43	3.50E-04
sludge SI-4.2 average	14	84	0	84	1.30E-03
sludge SI-4.2 fXAS1	14	85	0	85	1.40E-03
sludge SI-4.3 average	0	52	44	96	1.90E-03

R factor: Residual between fit and experimental data = $\Sigma[\mu_{exp} - \mu_{fit}]^2 / \Sigma[\mu_{exp}]^2$, where μ is the normalized absorbance.
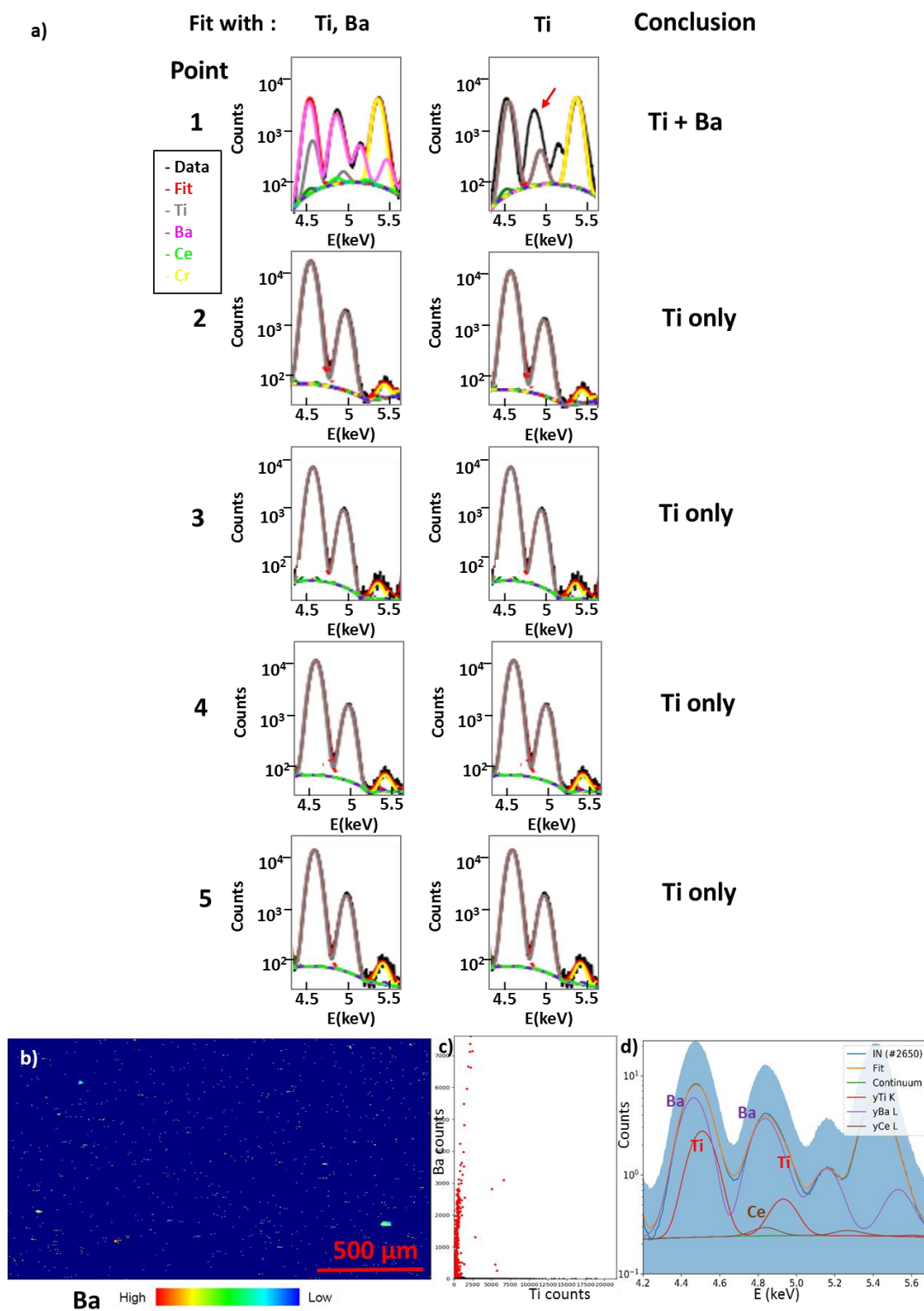
Figure S7. Investigation of the possible Ti-Ba-Ce association in sewage sludge. a) Deconvolution in the 4.5-5.5 KeV range of the XRF spectra extracted from regions 1 to 5 shown in Figure 2A-C with and without Ba. Red arrow indicates part of the spectrum that is not correctly fitted. b) Ba distribution in the sludge thin section. c) Scatter plot extracted from the Ba-rich spots in b). These spots represent only 0.6% (in area) of the total Ti-rich spots. d) XRF spectrum for the Ba-rich pixels in b). The blue area is the ±1x σ interval (meaning 1 x the standard deviation on all pixels included in the average), showing the variability between pixels. Peak deconvolution as compared to Figure S8 confirms that they contain much less Ti than the soil, and traces of Ce.
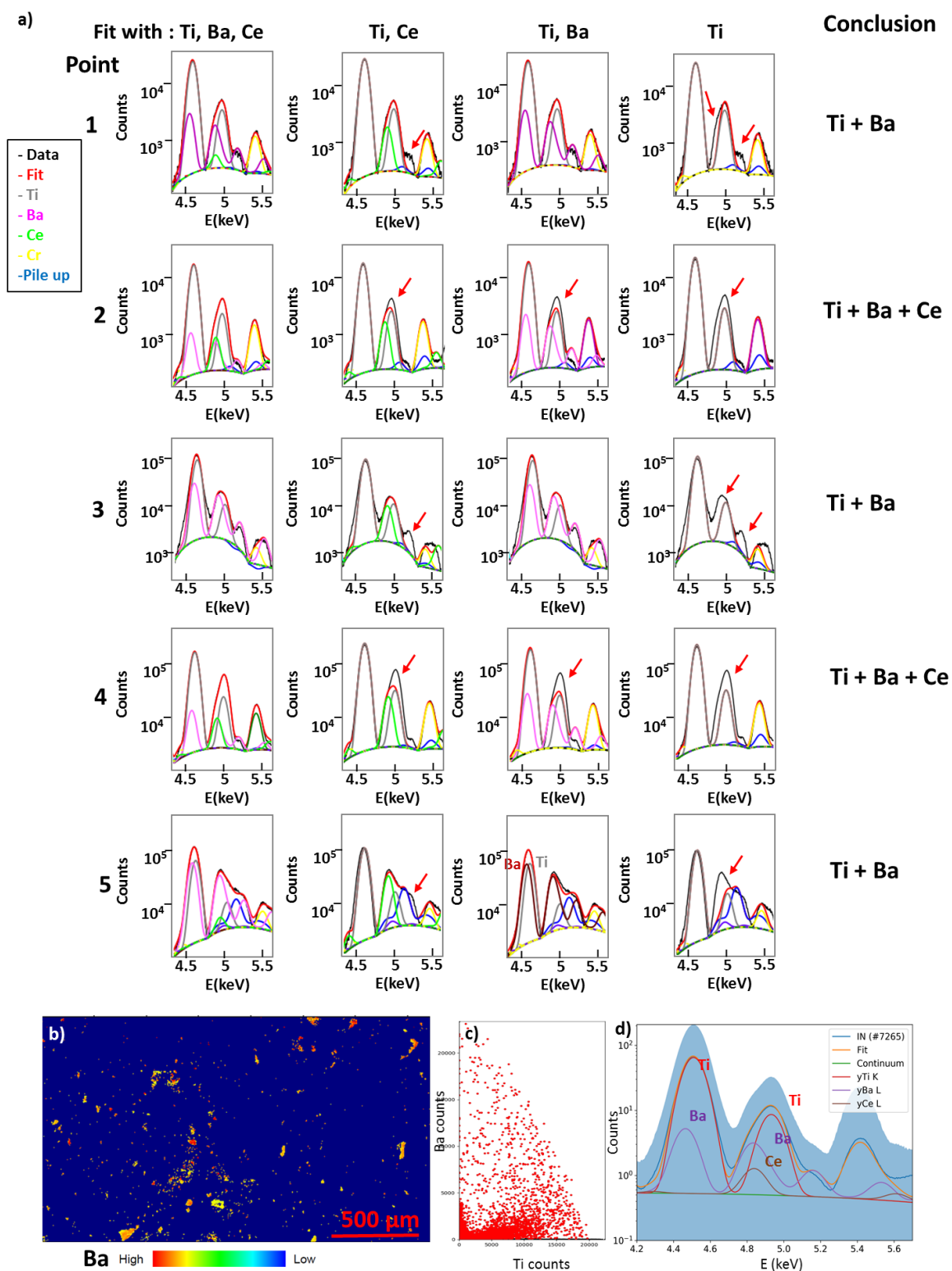
Figure S8. Investigation of the possible Ti-Ba-Ce association in sludge-amended soil. a) Deconvolution in the 4.5-5.5 KeV range of the XRF spectra extracted from regions 1 to 5 shown in Figure 2D-F with and without Ba and Ce. Red arrows indicate parts of the spectra that are not correctly fitted. For each spectrum, the conclusion on the presence of Ba and Ce is given on the right. b) Ba distribution in the amended soil thin section. The zones with strong overabsorption have been removed from the map and from the XRF analysis. c) Ba vs. Ti intensity scatter plot extracted from the Ba-rich spots in b). These spots represent 5.5% (in area) of the total Ti-rich spots. d) XRF spectrum for the Ba-rich spots in b). The blue area is the ±1x σ interval (meaning 1 x the standard deviation on all pixels included in the average), showing the variability between pixels. Peak deconvolution confirms that they contain Ba and Ti, and traces of Ce.
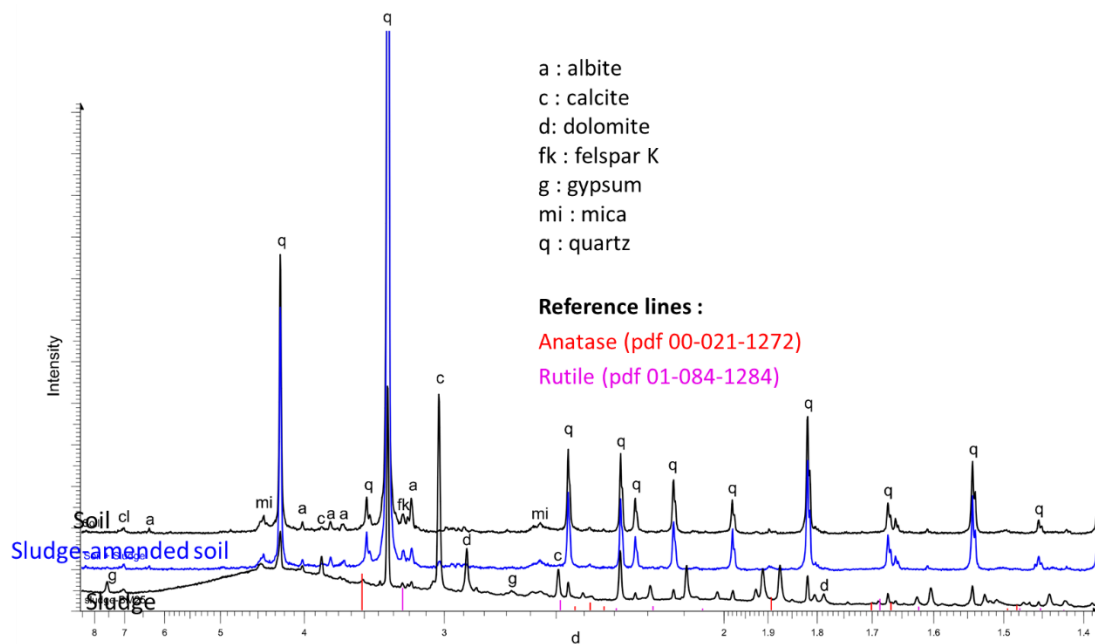
Figure S9. XRD patterns for the soil, sludge and sludge-amended soil.
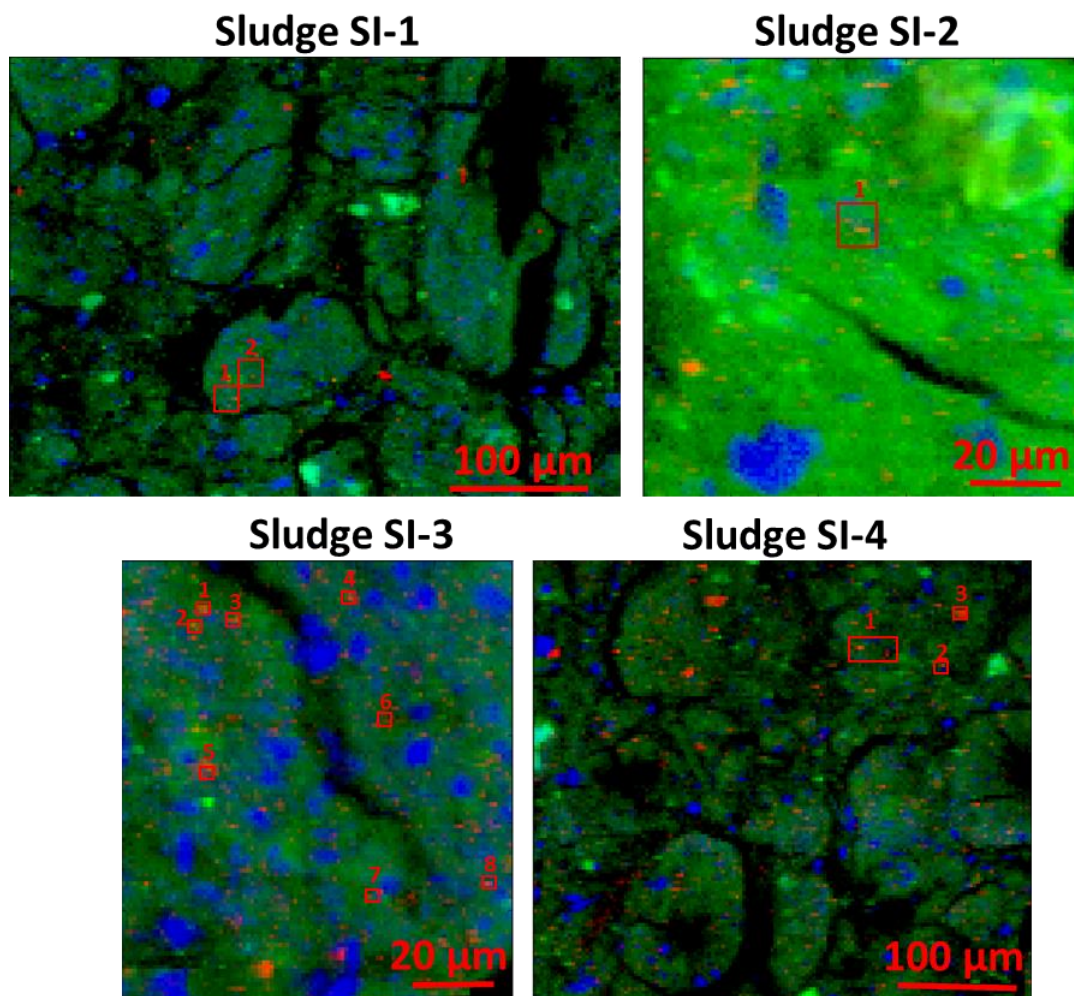
Figure S10. Tricolor µXRF maps for the sludge showing Ti(Red), S(green) and Si (blue). Incident energy: 5.2 keV. Maps have been calibrated so color intensities can be compared. Red squares indicates the areas where fXAS acquisitions were done, in order to extract Ti K-edge µXANES spectra.
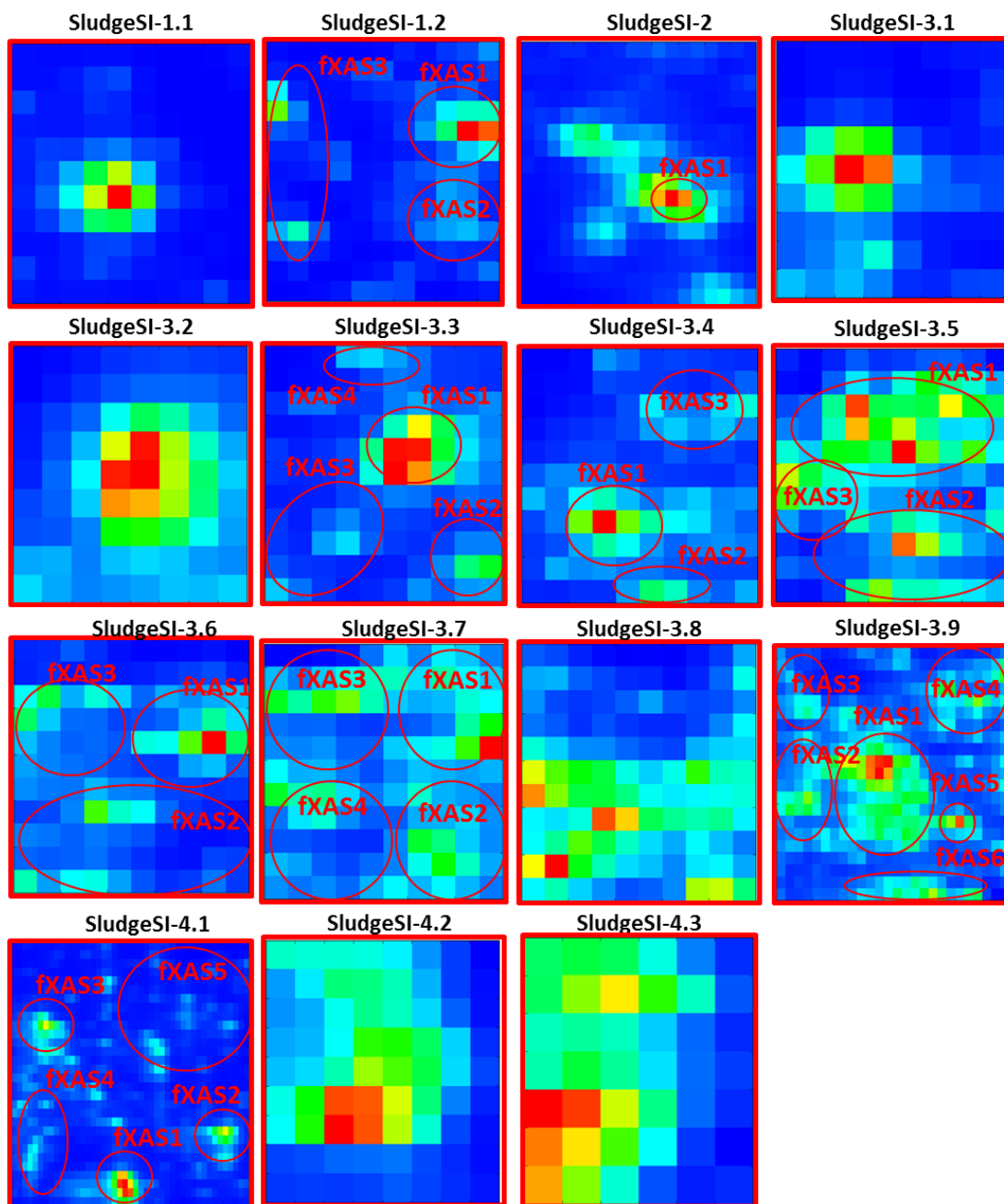
Figure S11. Close view of the fXAS zones shown in figure S10, presented as temperature maps for Ti. 1 pixel= 0.5 µm. Areas from which XANES spectra were extracted are highlighted by red ellipses. In other cases, the spectrum was extracted from the whole area.